A Single-Pool Model for Intracellular Calcium Oscillations and Waves in the *Xenopus laevis* Oocyte

Alireza Atri,* Jeff Amundson,‡ David Clapham,‡§ and James Sneyd*

*Department of Biomathematics, UCLA School of Medicine, Los Angeles, California, and Departments of ‡Physiology and Biophysics and §Pharmacology, Mayo Foundation, Rochester, Minnesota, USA

ABSTRACT We construct a minimal model of cytosolic free Ca^{2+} oscillations based on Ca^{2+} release via the inositol 1,4,5-trisphosphate (IP_3) receptor/Ca^{2+} channel (IP_3R) of a single intracellular Ca^{2+} pool. The model relies on experimental evidence that the cytosolic free calcium concentration ($[Ca^{2+}]_c$) modulates the IP_3R in a biphasic manner, with Ca^{2+} release inhibited by low and high $[Ca^{2+}]_c$ and facilitated by intermediate $[Ca^{2+}]_c$, and that channel inactivation occurs on a slower time scale than activation. The model produces $[Ca^{2+}]_c$ oscillations at constant $[IP_3]$ and reproduces a number of crucial experiments. The two-dimensional spatial model with IP_3 dynamics, cytosolic diffusion of IP_3 ($D_p = 300\ \mu m^2\ s^{-1}$), and cytosolic diffusion of Ca^{2+} ($D_c = 20\ \mu m^2\ s^{-1}$) produces circular, planar, and spiral waves of Ca^{2+} with speeds of 7–15 $\mu m \cdot s^{-1}$, which annihilate upon collision. Increasing extracellular $[Ca^{2+}]$ influx increases wave speed and baseline $[Ca^{2+}]_c$. A $[Ca^{2+}]_c$-dependent Ca^{2+} diffusion coefficient does not alter the qualitative behavior of the model. An important model prediction is that channel inactivation must occur on a slower time scale than activation in order for waves to propagate. The model serves to capture the essential macroscopic mechanisms that are involved in the production of intracellular Ca^{2+} oscillations and traveling waves in the *Xenopus laevis* oocyte.

INTRODUCTION

Changes in the concentration of cytosolic free calcium ($[Ca^{2+}]_c$) have been found to be responsible for the initiation and regulation of a variety of cellular functions including cellular proliferation, secretion, metabolic adjustments, and changes in gene expression (Berridge, 1993; Davis, 1992). The spatiotemporal patterns of $[Ca^{2+}]_c$ as a result of agonist stimulation are as diverse as the roles Ca^{2+} plays in different cells. The temporal pattern of $[Ca^{2+}]_c$ observed in a variety of cells includes oscillations or repetitive spiking (Berridge, 1993; Cobbold and Cuthbertson, 1990; Meyer and Stryer, 1991; Tsunoda, 1991). Some cells, most notably *Xenopus* oocytes, also exhibit interesting spatial patterns of $[Ca^{2+}]_c$, including propagating waves and target and spiral patterns (Lechleiter and Clapham, 1992). Ca^{2+} waves have also been observed in myocytes, astrocytes (Charles et al., 1991), hepatocytes (Meyer and Stryer, 1991), and airway epithelial cells (Sanderson et al., 1990; Boitano et al., 1992).

The exact function of the complex spatiotemporal patterns of Ca^{2+} is not yet understood. However, it is believed to be an efficient way of encoding information and transmitting the signal intracellularly (Lechleiter and Clapham, 1992). Oscillations may permit a smoothly graded input, such as percentage receptor occupancy, to be translated into a digital all-or-nothing signal in which the information is encoded in the pulse frequency (Tsien and Tsien, 1990). In this way, Ca^{2+} spikes, like action potentials, enable cells to use digital logic in transducing signals (Meyer and Stryer, 1991), thus increasing the signal-to-noise ratio. Ca^{2+} waves are used to propagate signals both within and between cells. Intracellular waves enable a whole cell to respond appropriately to a local stimulus, while intercellular waves propagate this signal to obtain a coordinated response from surrounding cells.

Although a number of models have been proposed, the underlying cellular mechanisms responsible for $[Ca^{2+}]_c$ oscillations and wave propagation remain undefined. It seems likely that the responsible mechanisms differ from one cell type to another.

It is of interest to us to understand the mechanisms underlying the complex spatiotemporal behavior of Ca^{2+} in the *Xenopus* oocyte. Although this behavior is wavelike in nature (Lechleiter and Clapham, 1992; Girard and Clapham, 1993; Camacho and Lechleiter, 1993; Parker and Yao, 1992), it is almost certainly the result of an underlying excitable/oscillatory temporal mechanism (Murray, 1989). Thus, in order to construct a realistic model of the spatiotemporal patterns of Ca^{2+} in the *Xenopus* oocyte, one must first construct a temporal model for oscillations.

A number of mathematical models, based on different theoretical models, have been proposed to account for intracellular $[Ca^{2+}]_c$ oscillations in a variety of cells. However, given current experimental evidence, none of the previous models serve to adequately describe Ca^{2+} oscillations and waves in the *Xenopus* oocyte.

In accordance with experimental evidence, all the models agree on the initial phase of this process. The binding of neurotransmitters or hormones to receptors linked via G-proteins (Davis, 1992) to phospholipase C (PLC) causes the breakdown of membrane-bound phosphotidylinositol-(4,5)-bisphosphate, producing two messengers, the lipid-soluble diacylglycerol (DAG) and the water-soluble IP_3 (Berridge, 1987; Berridge and Irvine, 1989; Peterson and

Received for publication 24 March 1993 and in final form 19 July 1993.

Address reprint requests to Dr. James Sneyd, Department of Biomathematics, UCLA School of Medicine, 10833 LeConte Avenue, Los Angeles, CA 90024-1766. email sneyd@kiwi.biomath.medsch.ucla.edu.

0006-3495/93/10/1727/13 $2.00

Wakui, 1990). IP_3 then releases Ca^{2+} from an IP_3-sensitive store, widely believed to be the endoplasmic reticulum (ER). The models can be categorized into two types, depending on whether they require oscillating $[IP_3]$ to drive the oscillations in $[Ca^{2+}]_c$. The first class requires oscillating $[IP_3]$ and includes (*a*) the IP_3-Ca^{2+} cross-coupling model of Meyer and Stryer (1991), which involves IP_3-induced Ca^{2+} release and Ca^{2+}-stimulated IP_3 formation, and (*b*) the agonist-receptor oscillator model of Cuthbertson and Chay (1991), which models interactions and feedback of the elements of the phosphatidylinositol (PI)-linked pathway and involves negative feedback of DAG-stimulated protein kinase C and subsequently IP_3 production. At present, it is not possible to measure $[IP_3]$ intracellularly with a high temporal resolution, and thus one cannot definitively say whether $[IP_3]$ oscillates during receptor activation. However, there is evidence that questions the significance of feedback on IP_3 production in the generation of Ca^{2+} oscillations in the *Xenopus* oocyte as well as in other cell types. Experiments in which oscillations were induced using myoinositol (1,4,5)trisphosphorothioate (IP_3S_3) in place of IP_3 (Lechleiter and Clapham, 1992; Peterson and Wakui, 1990) argue against the necessity for oscillating $[IP_3]$ to drive the $[Ca^{2+}]_c$ oscillations. Also, the spatiotemporal patterns of $[Ca^{2+}]_c$ in the *Xenopus* oocyte are the same regardless of whether IP_3 or IP_3S_3 is used to initiate the oscillations and waves (Lechleiter and Clapham, 1992; DeLisle and Welsh, 1992).

The second class of models does not require oscillations in $[IP_3]$ to drive the oscillations in $[Ca^{2+}]_c$; oscillations in $[Ca^{2+}]_c$ occur for appropriate and constant $[IP_3]$. The second class of models includes the following:

1: The Ca^{2+}-induced Ca^{2+} release (CICR) model (Goldbeter et al., 1990), a two-pool model that has cytosolic Ca^{2+} acting to release Ca^{2+} from an IP_3-insensitive store with ryanodine receptors. Although the ryanodine receptor plays an important role in many cells, immunological and biochemical experiments on the *Xenopus* oocyte (Parys et al., 1992) do not reveal the presence of the ryanodine receptor that is responsible for CICR in muscle and other cells (Endo et al., 1970; Fabiato, 1983; Tsien and Tsien, 1990).

2. The model of Somogyi and Stucki (1991), which involves one intracellular Ca^{2+} storage compartment with cooperative and positive feedback of Ca^{2+} on its own release through an IP_3-sensitive channel. This model is not consistent with experimental evidence, which shows that the IP_3R is modulated both positively and negatively by Ca^{2+} (Parys et al., 1992; Bezprozvanny et al., 1991; Iino, 1990; Finch et al., 1991; Parker and Ivorra, 1990; Iino and Endo, 1992).

3. The model of DeYoung and Keizer (1992) is a kinetic channel model of the IP_3R that represents the dynamics of the IP_3R as transitions of the channel's subunits through eight substates. Although an excellent channel model, this model is far from minimal and involves a set of nine coupled ordinary differential equations, which, by using a rapid equilibrium argument, may be simplified to a set of five.

There is also controversy regarding the mechanism of $[Ca^{2+}]_c$ wave propagation, and a number of qualitative models have been proposed. The models all contain positive feedback but differ on mechanisms and on whether Ca^{2+} or IP_3 is the propagating messenger. It has been proposed (Goldbeter et al., 1990; Girard et al., 1992; Sneyd et al., 1992) that the wave is propagated by Ca^{2+} diffusion and then amplified by CICR. Ehrenstein and FitzHugh (1986) and Meyer and Stryer (1991) propose that the wave is propagated by IP_3 diffusion through a positive feedback mechanism that involves Ca^{2+} activation of PLC, and Lechleiter and Clapham (1992) and others (Parys et al., 1992; DeLisle and Welsh, 1992) propose that wave propagation is controlled by IP_3-mediated Ca^{2+} release from the IP_3R but is modulated by the cytoplasmic concentration and diffusion of Ca^{2+}.

The goal of this work has been to integrate into a minimal model current knowledge regarding the important components of the cellular machinery that produce Ca^{2+} oscillations and waves in the *Xenopus* oocyte. The model for oscillations (the temporal model) should not only produce the features of observed oscillations but also be simple enough to elucidate the essential properties responsible for these phenomena. The temporal model, when spatially extended, should also reproduce the observed spatiotemporal behavior of Ca^{2+} in the *Xenopus* oocyte. Therefore, our model contains only one intracellular pool of Ca^{2+} that releases Ca^{2+} through the IP_3R. The IP_3R is assumed to be modulated by $[Ca^{2+}]_c$ in a biphasic manner, with Ca^{2+} release inhibited by low and high $[Ca^{2+}]_c$ and facilitated by intermediate $[Ca^{2+}]_c$. The model also separates the time scales of channel activation and inactivation, such that inactivation occurs on a slower time scale (Finch et al., 1991).

Ca^{2+} OSCILLATIONS

The model

A schematic of the model can be seen in Fig. 1. Binding of an agonist to a cell surface receptor initiates, through the PI-linked pathway, the production of IP_3 as well as DAG. IP_3 can then bind to an IP_3R of an internal Ca^{2+} pool to release Ca^{2+} from this pool. Cytosolic Ca^{2+} can then facilitate or inhibit further Ca^{2+} release, depending on which IP_3R Ca^{2+} binding domain it activates (see the Appendix for a derivation of the model). Ca^{2+} can also be extruded from the cytosol in a $[Ca^{2+}]_c$-dependent manner through reuptake by the pool or pumping to the extracellular medium. Meanwhile, a relatively small amount of Ca^{2+} is leaked into the cytosol from outside the cell.

The model equations are (see Appendix)

$$\frac{dc}{dt} = J_{\text{channel}} - J_{\text{pump}} + J_{\text{leak}} \tag{1}$$

$$\tau_n \frac{dn}{dt} = n_\infty(c) - n \tag{2}$$

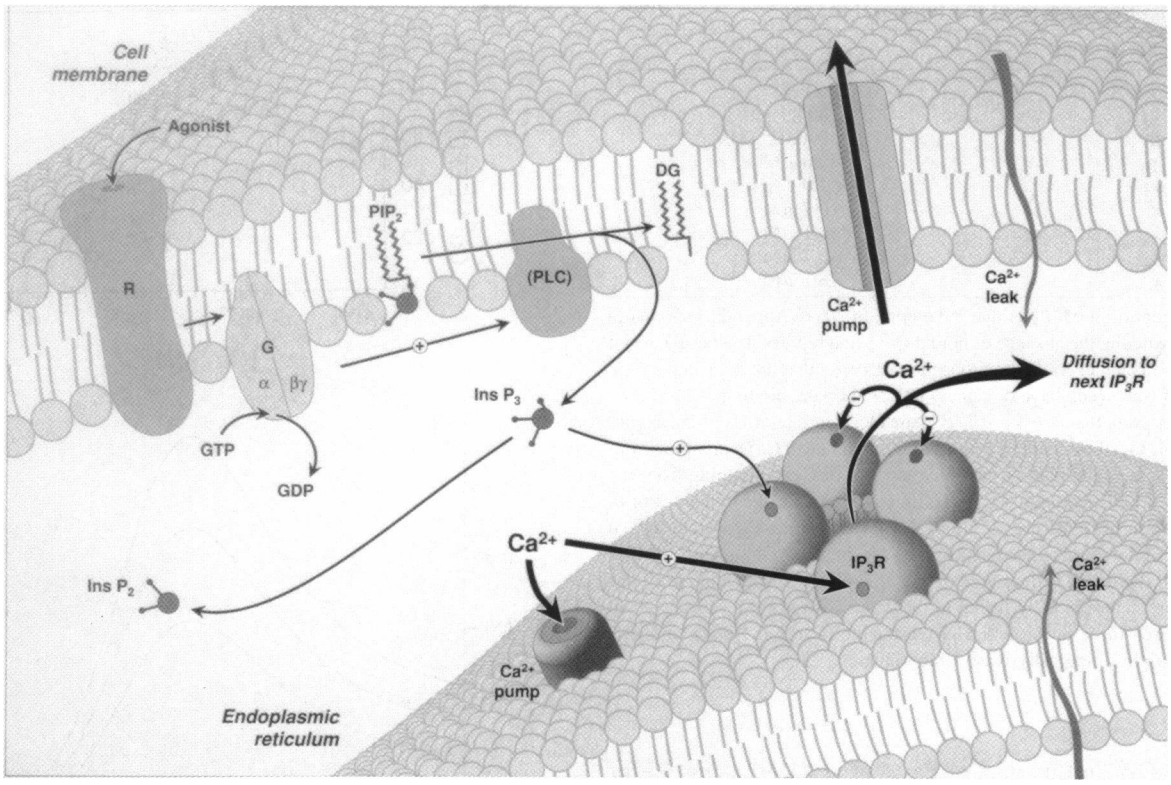

FIGURE 1 Schematic representation of the elements in the calcium wave model. Agonist-bound receptor (R) activates the G protein (G) by catalyzing the exchange of GTP for GDP. Phosphotidylinositol-(4,5)-bisphosphate (PIP_2) is hydrolyzed by its phosphodiesterase (PLC) to DAG and IP_3. IP_3 diffuses to binding sites on the IP_3 receptor (IP_3R), where it opens the calcium-permeable channel and allows calcium to flow out of the endoplasmic reticulum. Calcium coming out of the channel inactivates the channel (−) and diffuses to the next store site, where it enhances (+) the sensitivity of the IP_3R to IP_3. Calcium is taken back into the store via Ca^{2+} pumps. Calcium leaks into the cell and out of the ER through as yet undefined pathways, perhaps via the calcium pump protein itself. Reproduced with permission from J. Amundson and D. Clapham, *Curr. Opinions Neurobiol.* 3:375–382, Fig. 2.

where

$$J_{\text{channel}} = k_{\text{flux}}\mu([IP_3])n\left(b + \frac{V_1 c}{k_1 + c}\right) \tag{3}$$

$$J_{\text{pump}} = \frac{\gamma c}{k_\gamma + c} \tag{4}$$

$$J_{\text{leak}} = \beta \tag{5}$$

$$n_\infty(c) = 1 - \frac{c^2}{k_2^2 + c^2} \tag{6}$$

$$\mu([IP_3]) = \mu_0 + \frac{\mu_1[IP_3]}{k_\mu + [IP_3]}. \tag{7}$$

The variable c, in micromolar units, represents $[Ca^{2+}]_c$, and the dimensionless variable n represents the proportion of IP_3Rs that have not been closed by Ca^{2+}. Here, each J term represents a concentration flux and has units of $\mu M \cdot s^{-1}$. By assuming constant volume, each J term is simply related to the appropriate Ca^{2+} current, I; details are given in the Appendix. J_{channel} represents the Ca^{2+} flux through the IP_3R, J_{pump} represents the Ca_c^{2+} flux due to the $[Ca^{2+}]_c$-dependent pumping of Ca^{2+} out of the cytosol, and J_{leak} represents the Ca_c^{2+} flux due to Ca^{2+} leaking into the cytosol. The expression chosen for J_{pump} has little qualitative effect on model behavior, and thus we just used a simple expression. Incorporation of more detailed experimental information on the properties of the SERCA ATPase pumps (Lytton et al., 1992) is left for future work. Furthermore, we omit from the model any consideration of the lumenal Ca^{2+}. If the ER is locally depleted of Ca^{2+} during the passage of a wave or during an oscillation, one would expect that the concentration of Ca^{2+} in the ER would have a significant influence on oscillatory and wave properties. However, it is not yet known whether such depletion occurs in *Xenopus* oocytes. Further investigation of this point, and the construction of more detailed models, awaits further experimental work.

The function n_∞ represents the steady state of n as a function of c (since at steady state $dn/dt = 0$ from Eq. 2, it follows that $n = n_\infty$ at steady state), and $\mu([IP_3])$ is the proportion of IP_3Rs that have their IP_3 binding domain activated.

As described in the Appendix, the IP_3R is modeled in a way similar to that of the modeling of channel subunits in the Hodgkin-Huxley model of electrical impulse propagation in the nerve axon (Hodgkin and Huxley, 1952). Our variable n is directly analogous to the inactivation variable h in the Hodgkin-Huxley equations. Values for the model parameters are given in Table 1.

It is important to point out that the functional form of Eq. 3 was chosen so as to be consistent with the steady-state

TABLE 1 Parameters of the temporal model

Parameter	Value
b	0.111
V_1	0.889
β	0–0.02 $\mu M \cdot s^{-1}$
γ	2.0 $\mu M \cdot s^{-1}$
τ_n	2.0 s
k_1	0.7 μM
k_γ	0.1 μM
k_2	0.7 μM
k_{flux}	8.1 $\mu M \cdot s^{-1}$

b is the proportion of IP_3Rs that have domain 2 (see Appendix) spontaneously activated in the absence of bound Ca^{2+} and represents a basal current through the channel. V_1 is the proportion of IP_1Rs that are activated by the binding of Ca^{2+} (i.e., have domain 2 activated by the binding of Ca^{2+}; see Appendix). Note that $b + V_1 = 1$. β is the constant rate of Ca^{2+} influx into the cytosol from the outside. γ is the maximmum rate of Ca^{2+} pumping from the cytosol. k_γ is the $[Ca^{2+}]_c$ at which the rate of Ca^{2+} pumping from the cytosol is at half-maximum. τ_n is the time constant for the dynamics of n, the proportion of IP_3Rs not closed by Ca^{2+} (i.e., the time constant for the activation of domain 3; see Appendix). k_{flux} is the maximum total Ca^{2+} flux through all IP_3Rs and is described in more detail in the Appendix. b, V_1, k_1, and k_2 were determined by fitting to the data of Parys et al. (1992). γ and k_γ are chosen to be physiologically reasonable (Carafoli, 1987), and β is varied in a physiologically reasonable range.

channel Ca^{2+} efflux data of Parys et al. (1992) (Fig. 2) for the IP_3R from *Xenopus* oocytes. Also, μ_0 and μ_1 are chosen such that when $[IP_3]$ is low $[Ca^{2+}]_c$ is low and nonoscillatory, and when $[IP_3]$ is high $[Ca^{2+}]_c$ is elevated and nonoscillatory. Thus, for a range of agonist stimulations between these two levels, the steady-state $[Ca^{2+}]_c$ is oscillatory (Fig. 3). This representation of $\mu([IP_3])$ does not qualitatively affect the results and only serves to translate them in terms of $[IP_3]$. Since oscillations occur at constant $[IP_3]$, we need not consider IP_3 dynamics in the model for oscillations. Thus, in this section μ will be treated as a parameter that may be held fixed at any desired level between 0 and 1. In mathematical terms, μ is treated as the bifurcation parameter. However, IP_3 dynamics is important in the spatial propagation of Ca^{2+}, and thus the dependence of μ on $[IP_3]$ is included in the extended (spatial) model.

Modeling of the Ca^{2+} flux through the IP_3R in this manner is simply a macroscopic representation capturing the essence of other channel models (DeYoung and Keizer, 1992). In fact, the model presented here is very similar to a simplification of the DeYoung and Keizer model (Keizer and DeYoung, 1993). It is interesting that two very different approaches (a physical as opposed to a phenomenological channel model) give essentially the same result. A key feature of both models is the separation of the time scales of $[Ca^{2+}]_c$-dependent activation and inactivation of the channel, with inactivation occurring more slowly than activation, which is supported by Finch et al. (1991), who show that cytosolic Ca^{2+}, at physiological concentrations, rapidly activates and more slowly inactivates IP_3-induced Ca^{2+} release. Thus, choosing $\tau_n > 1$ s serves to accelerate activation compared to inactivation. We assume that channel activation by Ca^{2+} is instantaneous.

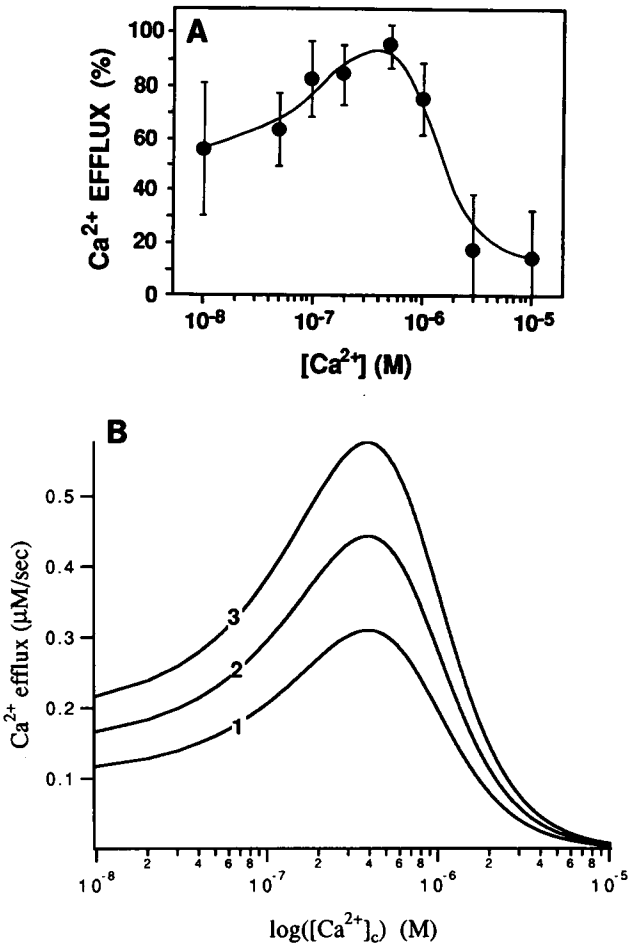

FIGURE 2 (*A*) Steady-state efflux of Ca^{2+} from the IP_3R (as a percentage of maximum) versus $[Ca^{2+}]_c$. Figure taken from Parys et al. (1992) showing data from *Xenopus* oocytes. (*B*) Model simulations of Ca^{2+} flux versus $[Ca^{2+}]_c$ for different $[IP_3]$. Different curves correspond to $\mu = 0.117$ (*curve 1*), 0.167 (*curve 2*), and 0.217 (*curve 3*). Note that the experimental curve measures the Ca^{2+} efflux as a percentage of the total Ca^{2+} in the pool, which is slightly different from the theoretical curves, which measure the Ca^{2+} flux through the receptor. Although a direct quantitative comparison is therefore inappropriate, the experimental data may be used as a guide for the construction of the theoretical steady-state curve.

Characteristics of oscillations and comparisons with experiments

Analysis of the model shows that, under certain physiological conditions, the model exhibits oscillations for an intermediate range of $[IP_3]$. For an $[IP_3]$ not in this oscillatory range, a stable steady state of $[Ca^{2+}]_c$ (c_{ss}) exists, which increases with increased $[IP_3]$ (thus with increased μ). At high $[IP_3]$, the system reaches a stable steady state characterized by a sustained elevated $[Ca^{2+}]_c$ (Fig. 3). Such qualitative behavior has been observed in a variety of cells (Lechleiter and Clapham, 1992; Berridge and Irvine, 1989; Cuthbertson, 1989; Harootunian et al., 1989; Rooney et al., 1990). Note that oscillations occur at a fixed $[IP_3]$.

The parameters used in the model are given in Table 1. For these parameter values, oscillations occurred for $0.578 \leq$

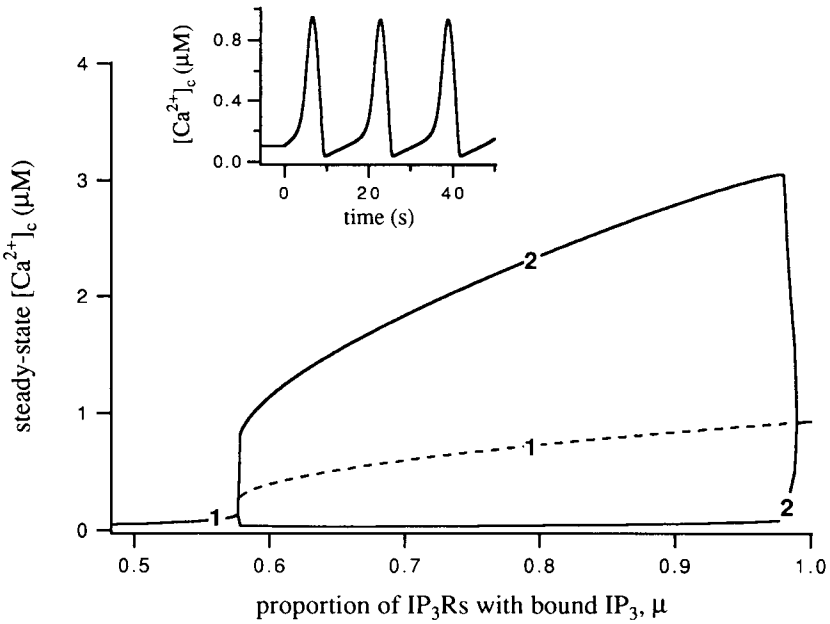

FIGURE 3 Bifurcation diagram for the model showing the steady-state $[Ca^{2+}]_c$ (*curve 1*) versus the bifurcation parameter, μ, which represents the proportion of IP_3Rs that have IP_3 bound (i.e., have domain 1 activated; see Appendix). In the oscillatory range of μ ($0.578 \leq \mu \leq 0.988$) the maximum and minimum amplitude of oscillations are represented by curve 2. The steady-state curve was found by setting the derivatives of c and n to zero and solving for c. The dashed line represents an unstable steady state. (*Inset*) Oscillations in $[Ca^{2+}]_c$ produced by raising the level of agonist stimulation, μ, to 0.583 at time 0, for a cell initially at a steady-state $[Ca^{2+}]_c$ of 102 nM. The minimum value of $[Ca^{2+}]_c$ during the oscillations is approximately 40 nM. This curve was obtained by numerical integration of the model equations.

$\mu \leq 0.988$, which corresponds to 120 nM $\leq c_{ss} \leq$ 910 nM. The model exhibits excitable behavior at pre-oscillatory stimulation levels. A suprathreshold Ca^{2+} pulse results in a transient yet substantial excursion from the steady state. This mimics the behavior of CICR yet is the result of the bell-shaped Ca^{2+}-dependent dynamics of the IP_3R and, to a lesser extent, the lag in inactivation compared to activation.

In most simulations a value of 0 was used for β, the extracellular rate of Ca^{2+} leakage into the cytosol. This was done to simulate the experimental conditions in which there was little or no extracellular Ca^{2+} present when oscillations and waves were induced (Lechleiter and Clapham, 1992).

Amplitude, period, and latency of oscillations

In most preparations, including those of *Xenopus* oocytes, the frequency of oscillations increases with increased agonist stimulation, whereas the amplitude remains relatively constant within a wide range of stimulation. With the cell in a nonoscillatory steady state, a transient of IP_3 is used to induce $[Ca^{2+}]_c$ oscillations. The time from the release of the IP_3 to the appearance of the first $[Ca^{2+}]_c$ peak is termed the *latency* of the oscillations. Latency has been observed to decrease toward a final plateau with increased stimulation. Figs. 3 and 4 show the relationship between amplitude, period, and latency in our model. These results are in qualitative agreement with the observed behavior in many cells, including the *Xenopus* oocyte (Lechleiter and Clapham, 1992; Berridge and Irvine, 1989; Harootunian et al., 1989; Parker and Ivorra, 1992; Berridge and Galione, 1988; Quin et al., 1988; Sage and Rink, 1987).

Latency correlates with period

Experimental observations indicate that latency is a linear function of the period (Rooney et al., 1990). Our model gives reasonable agreement with the experimental results, giving a least-square fit line with slope 2 to the period versus latency points (Fig. 4).

Ca^{2+} superfusion protocol

Using a superfusion protocol, Finch et al. (1991) investigated the dependence of IP_3-induced Ca^{2+} efflux on $[Ca^{2+}]_c$. At a fixed $[IP_3]$, $[Ca^{2+}]_c$ was stepped up and held fixed for 2 s, and the resulting net Ca^{2+} efflux was measured. The protocol was repeated for different steps of $[Ca^{2+}]_c$. They presented their efflux amount as a percentage of the total initial amount of Ca^{2+} release by the vesicle. In our simulations $[Ca^{2+}]_c$ was stepped up and held fixed for 10 s (since it did not reach a steady state in 2 s), and the rate of efflux was measured by the net channel flux, $J_{channel}$ (Fig. 5). Simulation results, in both the form and characteristics of the rise and fall of the efflux rate, give good qualitative agreement with their experiments. In both the experimental and simulation results, higher steps of $[Ca^{2+}]_c$ produce higher peaks, and these fall at a faster rate. Also, in the simulation results, notice the manifestation of the biphasic steady-state flux curve toward the later time points, with the curves corresponding to intermediate $[Ca^{2+}]_c$ (150–650 nM) possessing larger Ca^{2+} efflux rates than those corresponding to other $[Ca^{2+}]_c$. Due to the vertical scaling of figure of Finch et al., the manifestation of the steady-state biphasic curve may not be readily apparent in their data.

Paired-IP_3 pulse protocol

Parker and Ivorra (1990) used light-flash photolysis of caged IP_3 to generate transients of free IP_3 in the cytoplasm of *Xenopus* oocytes. The resulting liberation of Ca^{2+} from intracellular stores was monitered by recording Ca^{2+}-activated

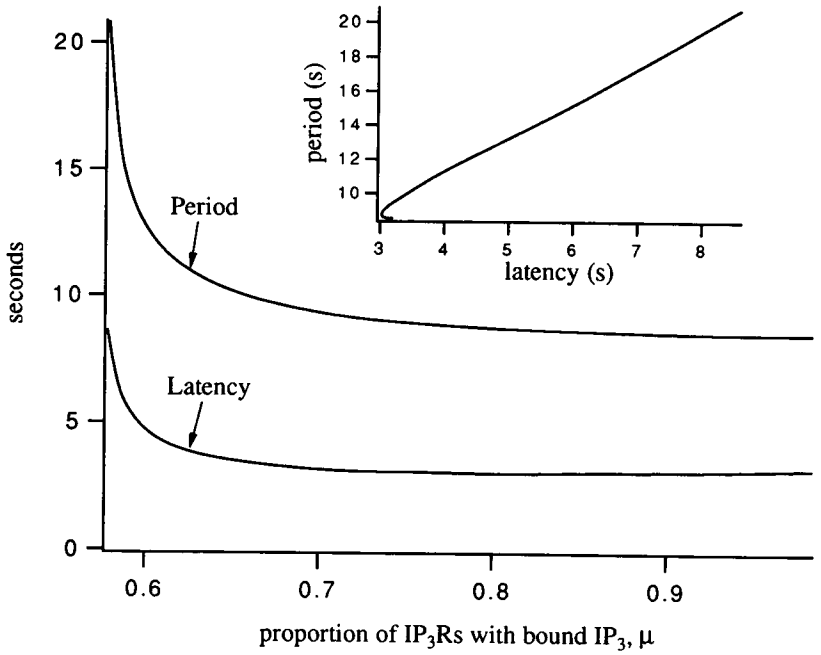

FIGURE 4 Period and latency of oscillations versus proportion of IP_3Rs with IP_3 bound, μ. (*Inset*) Period versus latency of the oscillations. The least-squares best-fit line through the points has a slope of 2.

membrane currents and by the use of the fluorescent Ca^{2+} indicator fluo-3. The experiments were composed of light pulses of equal intensity and duration (0.05 to 0.1 ms), with the time interval between the paired pulses serving as a variable. In each pair the response to the first pulse served as the control, and the data were presented as the interval between pulses versus response size (percentage of control response). Fig. 6 *a* shows their results as measured with fluo-3. Their measurement exhibits an inhibition of Ca^{2+} release in the 2–5-s range, which gradually diminishes. The transient in free IP_3 was simulated with a step increase in μ for a duration of 0.14 ms. As can be seen from Fig. 6 *b*, our simulations exhibit an inhibition of Ca^{2+} release in the 2.5–5-s range and agree qualitatively with the results of Parker and Ivorra.

IP_3 and Ca^{2+} flash photolysis protocol

Iino and Endo (1992) analyzed the kinetics of IP_3-induced Ca^{2+} release following flash photolysis of caged IP_3 or Ca^{2+} to demonstrate that Ca^{2+}-dependent immediate feedback control is an important determinant of the time course of Ca^{2+} release in smooth muscle cells. In order to measure Ca^{2+} release into the cytosol, Ca^{2+} uptake by the ER was eliminated. In one experiment the dependence of Ca^{2+}

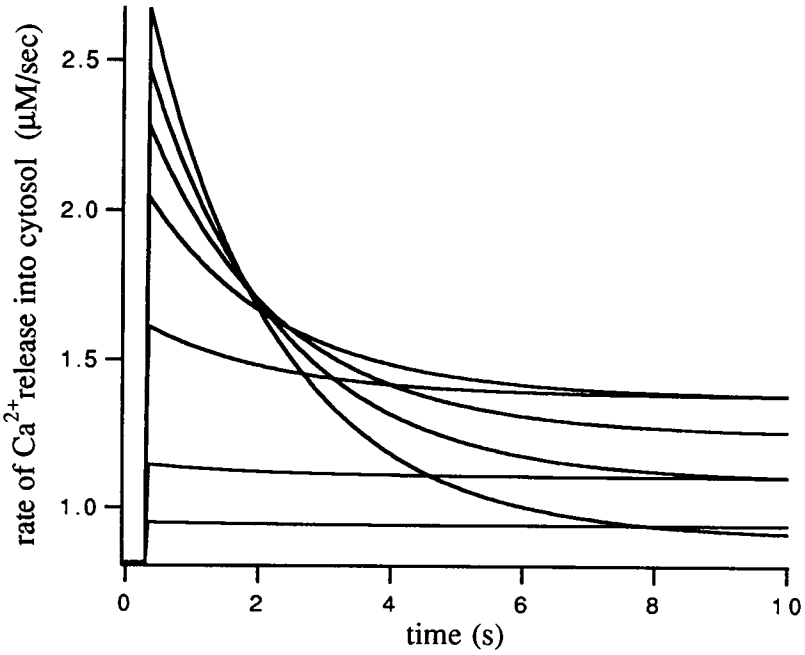

FIGURE 5 Dependence of IP_3-induced Ca^{2+} efflux on $[Ca^{2+}]_c$. Model simulation of Finch et al.'s protocol showing the rate of Ca^{2+} release into the cytosol versus time. $\mu = 0.217$, and $[Ca^{2+}]_c$ is held fixed for 10 s. The different curves (as the peaks increase) correspond to $[Ca^{2+}]_c$'s (nM) of 100, 150, 300, 500, 650, 800, and 1000.

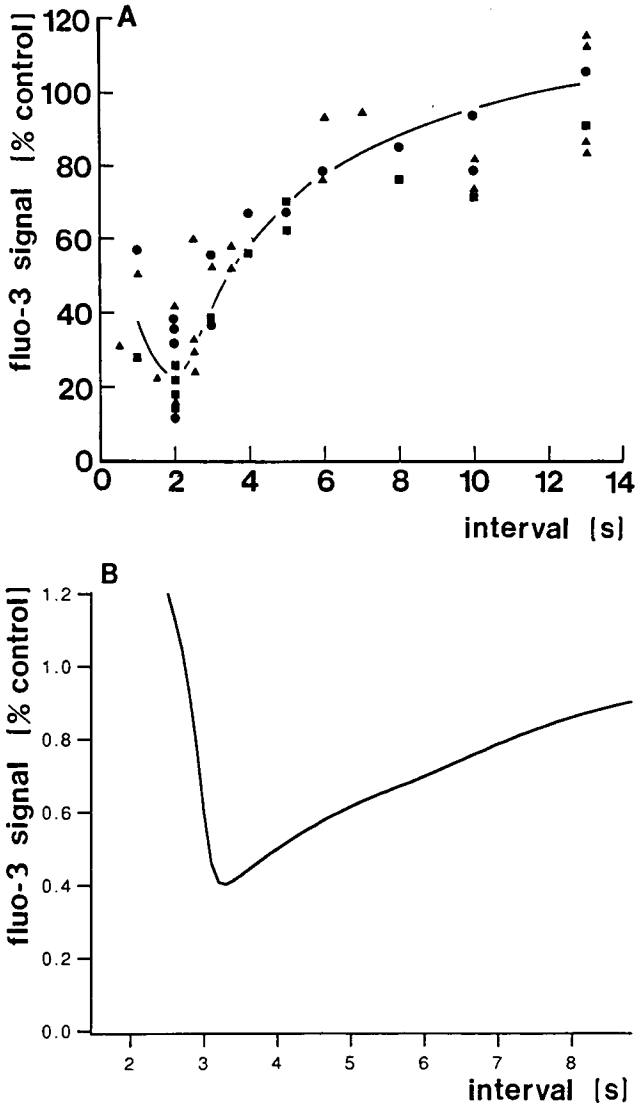

FIGURE 6 Time course of facilitation and depression of Ca^{2+} release measured with paired pulses of IP_3. (*A*) Figure from Parker and Ivorra (1990) showing response size (percentage of control), as measured by fluo-3 signal, versus interval between pulses. Paired pulses are identical in intensity and duration. For different pairs of pulses the duration of the pulses varied from 5 to 100 ms. (*B*) Simulation result for identical pulses of duration 14 ms and intensity $\mu = 0.967$.

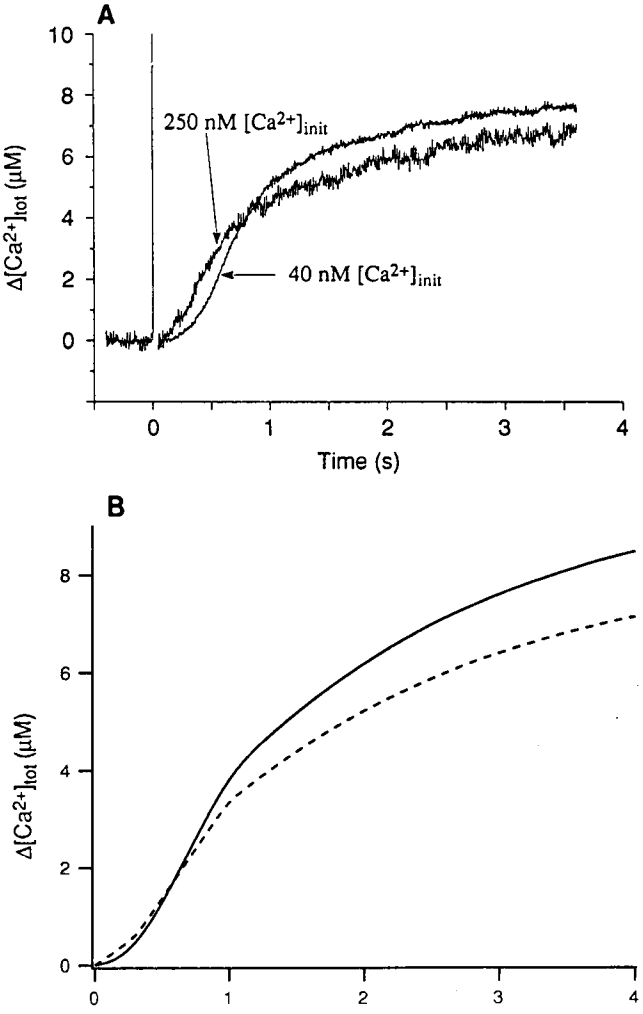

FIGURE 7 Dependence of Ca^{2+} release on the pre-flash $[Ca^{2+}]_c$ ($[Ca^{2+}]_{init}$). (*A*) Figure from Iino and Endo (1992) showing the time course of Ca^{2+} release in the presence of 100 μM fluo-3 for $[Ca^{2+}]_{init}$ of 40 nM and 250 nM with no Ca^{2+} uptake. The difference between $[Ca^{2+}]_c$ and $[Ca^{2+}]_{init}$ ($\Delta[Ca^{2+}]_{tot}$) is plotted versus time (s). Reproduced with permission from *Nature (Lond.)*. 360:76–78. © 1993 Macmillan Magazines Limited. (*B*) Simulation results for $[Ca^{2+}]_{init}$ of 48 nM ($\mu = 0.48$) (——) and 400 nM ($\mu = 0.603$) (- - - -). $\Delta[Ca^{2+}]_{tot}$ is plotted versus time. The flash releasing IP_3 is simulated by a step increase of μ to 1.0 for a period of 500 ms starting at 0.5 s, and the pump is disabled ($\gamma = 0$).

release on pre-flash $[Ca^{2+}]_c$ is investigated. When caged IP_3 is photolysed at a pre-flash $[Ca^{2+}]_c$ ($[Ca^{2+}]_{init}$) that is near the peak of the biphasic Ca^{2+} dependence of IP_3-induced Ca^{2+} release, the lag time in Ca^{2+} release becomes shorter, the initial rate of Ca^{2+} release greater, and the slowing of Ca^{2+} release starts earlier than when a much lower $[Ca^{2+}]_{init}$ is used (Fig. 7 *a*). Model simulations of this protocol give excellent qualitative agreement with the experiments (Fig. 7 *b*). The release of IP_3 was simulated by a step increase of μ for a period of 100–500 ms, the pump was disabled by setting $\gamma = 0$, and the difference between $[Ca^{2+}]_c$ and $[Ca^{2+}]_{init}$ ($\Delta[Ca^{2+}]_{tot}$) is measured and plotted versus time.

Ca^{2+} WAVES

The Model

We extend the model to two spatial dimensions and add cytosolic diffusion and breakdown of IP_3, and cytosolic diffusion of Ca^{2+}. The model equations are

$$\frac{\partial P}{\partial t} = D_p(P_{xx} + P_{yy}) - k_p P \tag{8}$$

$$\frac{\partial c}{\partial t} = D_c(c_{xx} + c_{yy}) + k_{flux}\mu(P)n\left(b + \frac{V_1 c}{k_1 + c}\right) - \frac{\gamma c}{k_\gamma + c} + \beta \tag{9}$$

$$\tau_n \frac{dn}{dt} = n_\infty(c) - n \tag{10}$$

where

$$\mu(P) = \mu_0 + \frac{\mu_1 P}{k_\mu + P}, \tag{11}$$

and $n_\infty(c)$ is the same as before (Eq. 6). P is $[IP_3]$, while D_c and D_p are the cytosolic diffusion coefficients of Ca^{2+} and IP_3, respectively. Since IP_3 dynamics are important to the spatial model, an IP_3 equation (Eq. 8) is included that represents the rate of change of $[IP_3]$ in terms of diffusion and linear breakdown of IP_3. Furthermore, the proportion of IP_3Rs that are activated by IP_3 (μ), which can serve to represent the level of agonist stimulation, is now appropriately represented as a function of $[IP_3]$ (Eqs. 7 and 11). It is important to understand that the form of $\mu(P)$ is dependent on cell type and functions to control the range of IP_3 concentrations for which oscillations are observed. For instance, a larger Hill coefficient would serve to decrease the range of $[IP_3]$ for which oscillations are observed but would not affect the qualitative behavior of the model, affecting only the quantitative translation of the results in terms of $[IP_3]$. Similarly, our value for k_μ is somewhat arbitrary. As can be easily seen, P may be rescaled throughout by k_μ without changing the model equations. Setting $k_\mu = 4$ μM results in Ca^{2+} oscillations over a physiologically reasonable range of IP_3 concentrations. Unless otherwise specified, the parameters used in the simulations are listed in Table 2.

A range of values was used for k_p, the linear breakdown rate of IP_3. This was done to simulate both experiments with IP_3 and with IP_3S_3, which is not degraded (thus, we use $k_p = 0$ to simulate this). The intracellular half-life of IP_3 has been estimated to be about 4 s (Berridge, 1987), which gives a $k_p = 0.17\ s^{-1}$. The values of 300 and 20 $\mu m^2 \cdot s^{-1}$ for D_p and D_c, respectively, were chosen to be consistent with recent experimental estimates (Albritton et al., 1992).

As in experiments that examine the IP_3 dependence and Ca^{2+} dependence of intracellular Ca^{2+} wave propagation, intracellular release of IP_3 or Ca^{2+} was used to generate Ca^{2+} waves. We simulate this by elevating $[IP_3]$ or $[Ca^{2+}]_c$ in a region of the cell and holding this concentration fixed, in that region, for a short amount of time (from a few hundred milliseconds to a few seconds in different simulations). Our simulation domain had dimensions of 250 × 250 μm in some simulations and 500 × 500 μm in other simulations. As expected, similar results were obtained regardless of the domain size. The initial $[IP_3]$ and $[Ca^{2+}]_c$ for the rest of the domain is set according to the experimental protocol being simulated, which for many experiments is their steady-state values of 0 and ~100 nM, respectively. No-flux conditions are chosen to simulate the cell boundaries.

Most of our simulations are performed with no influx of Ca^{2+} from the outside ($\beta = 0$). However, the dependence of wave speed and baseline $[Ca^{2+}]_c$ on the amount of Ca^{2+} influx into the cytosol from the outside was investigated by varying β, the constant influx rate of Ca^{2+}, in some simulations. Also, the effect of a $[Ca^{2+}]_c$-dependent Ca^{2+} diffusion coefficient (Albritton et al., 1992) on the waves produced by the model was investigated.

TABLE 2 Additional parameters of the spatiotemporal model

Parameter	Value
D_p	300 $\mu m^2 \cdot s^{-1}$
D_c	20 $\mu m^2 \cdot s^{-1}$
k_p	0–0.2 s^{-1}
k_μ	4.0 μM
μ_0	0.567
μ_1	0.433

D_p and D_c are the cytosolic diffusion coefficients of IP_3 and Ca^{2+}, respectively, and are consistent with recent experimental estimates (Albritton et al., 1992). k_p is the linear rate of IP_3 breakdown $k_p = 0$ is used to stimulate experiments with IP_3S_3, and a $k_p \approx 0.17\ s^{-1}$ is consistent with experimental evidence (Berridge, 1987) for the cytosolic half-life of IP_3. μ_0 is the proportion of IP_3Rs that are activated at $[IP_3] = 0$ μM (i.e., have domain 1 activated in the absence of bound IP_3; see Appendix), and μ_1 is the proportion of IP_3Rs that are activated by bound IP_3 (i.e., have domain 1 activated with the binding of IP_3; see Appendix). Note that $\mu_0 + \mu_1 = 1$. Refer to the text for more discussion of these parameters.

RESULTS

The most interesting prediction of the model is unless Ca^{2+}-dependent inactivation of the IP_3R occurs on a time scale at least twice as slowly (i.e., $\tau_n \geq 2$ s) as Ca^{2+}-dependent activation of the IP_3R, a propagating Ca^{2+} wave will not be generated. Note that τ_n also influences the speed of recovery from inactivation; as τ_n increases, the width of the wave front increases also.

Another characteristic of the Ca^{2+} waves produced by the model is that, regardless of the method by which a wave is initiated, it behaves in the manner of waves in a classic excitable medium. Therefore, colliding waves annihilate because of the existence of a refractory period immediately behind the wave. Meanwhile, waves initiated from different foci may also fuse to form a joint wavefront. Fig. 8 shows a typical profile for a traveling wave produced by the model. The relationship between the wave speed, the diffusion coefficents of Ca^{2+} and IP_3, and the rise time of the wave front is discussed in detail in Sneyd and Kalachev (1993). Suffice it to say here that, without detailed consideration of Ca^{2+} buffering, it is inappropriate to compare the detailed structure of the wave front to experimental results; only more general qualitative results may be obtained.

Planar and circular waves initiated by IP_3 release

Lechleiter and Clapham (1992) obtained propagating planar waves of Ca^{2+} by photoreleasing IP_3 in a narrow band within the *Xenopus* oocyte. We simulate these experiments by elevating $[IP_3]$ and holding this concentration fixed for 300 milliseconds, on one side of the cell. A propagating planar wave of Ca^{2+} emanates from this region and travels across the cell (not shown). The speed of the wave is dependent, among other things, on the square root of the cytosolic diffusion coefficient of Ca^{2+}, $\sqrt{D_c}$. As D_c was varied from 20

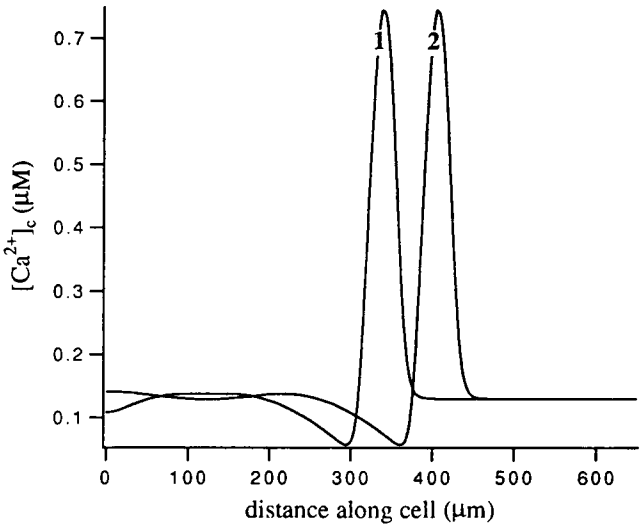

FIGURE 8 Propagation of a traveling wave of Ca^{2+} (in one dimension) for a simulation with cytosolic diffusion of Ca^{2+} (D_c = 50 $\mu m^2\ s^{-1}$) and μ held constant across the whole cell (μ = 0.578). $[Ca^{2+}]_c$ is plotted versus distance along the cell. A wave was started using a step increase of $[Ca^{2+}]_c$ to 0.9 μM on the left side of the domain while the rest of the domain is at a steady-state $[Ca^{2+}]_c$ of 130 nM. The waves correspond to times of 28 (curve 1) and 34 (curve 2) s. The wave is propagating at approximately 11 $\mu m \cdot s^{-1}$.

to 50 $\mu m^2 \cdot s^{-1}$ the wave speed varied from 7 to 11 $\mu m \cdot s^{-1}$. These wave speeds are in good agreement with experimental measurements, which range from 5 to 25 $\mu m \cdot s^{-1}$ (Girard et al., 1992; Girard and Clapham, 1993). If the initial elevation of $[IP_3]$ is high enough or the rate of breakdown of IP_3, k_p, is low enough, then subsequent Ca^{2+} waves will be initiated from the same region. This is because, under these conditions, $[IP_3]$ will remain high enough in that region for enough time to initiate subsequent wave activity. Conversely, if IP_3 breakdown is fast enough, elevation of IP_3 in a local region fails to initiate a propagating wave because of the dispersal and degradation of IP_3 (Fig. 9).

The general scenario for IP_3-induced Ca^{2+} wave propagation goes like this: the initial bolus of IP_3 initiates Ca^{2+} release through the IP_3Rs in the region of high $[IP_3]$. Meanwhile, IP_3 primes other IP_3Rs (i.e., activates domain 1) as it diffuses rapidly outward and initiates some release of Ca^{2+}, since at low $[Ca^{2+}]_c$ domain 2 is activated and domain 3 is inactivated (see Appendix). The released Ca^{2+} diffuses more slowly and, upon reaching the primed IP_3Rs, initiates greater Ca^{2+} release by activating domain 2. In this way an outwardly propagating Ca^{2+} wave is generated. When $[Ca^{2+}]_c$ starts to peak, $[Ca^{2+}]_c$ activates domain 3 on the IP_3R, inhibiting Ca^{2+} release through the channel. With many channels inactivated, Ca^{2+} release drops, and the pumps remove the cytosolic Ca^{2+} back into the intracellular pool and to the outside of the cell (the latter is of little consequence for regions more toward the inside of the cell and away from the plasma membrane). As a result $[Ca^{2+}]_c$ begins to drop and a waveback is created. The region behind the waveback experiences a classic refractory period, which is enhanced by channel inactivation occurring on a slower time scale than activation.

Planar and circular waves initiated by Ca^{2+} release

We simulate experiments in which a large amount of IP_3S_3 is used to keep $[IP_3S_3]$ almost constant across the whole cell while a locally elevated $[Ca^{2+}]_c$ produces a propagating Ca^{2+} wave. We thus elevate $[IP_3]$ and keep it constant throughout the cell while a region of elevated $[Ca^{2+}]_c$ (elevated for a few hundred milliseconds to a few seconds) becomes the initiating site for a propagating wave of Ca^{2+}. Fig. 10 *a* shows an observed planar Ca^{2+} wave in the *Xenopus* oocyte, and Fig. 10 *b* shows a planar wave obtained from a model simulation.

In this scenario, because of a significant and constant $[IP_3]$ throughout the cell, most IP_3Rs are already primed. The elevation of $[Ca^{2+}]_c$ then initiates Ca^{2+} release and wave propagation through Ca^{2+} activation of the IP_3R and diffusion of Ca^{2+}.

Spiral waves

Spiral waves can arise as part of a wave front encounters a refractory region and starts to bend around itself. Once this bending is initiated, the curvature dependence of the velocity of the wavefront can maintain spiral wave propagation (Keener, 1986; Zykov, 1980). It must be pointed out that the curvature dependence of the wave velocity depends on the nature of the excitable media (Sneyd and Atri, 1993).

We can obtain a propagating spiral wave by having part of a Ca^{2+} wave encounter a refractory region where $[Ca^{2+}]_c$ is below steady-state levels for a short time. The rest of the cell is initially at a steady-state level of $[Ca^{2+}]_c$, while $[IP_3]$ is constant throughout the cell. Fig. 11 (*a* and *b*, respectively)

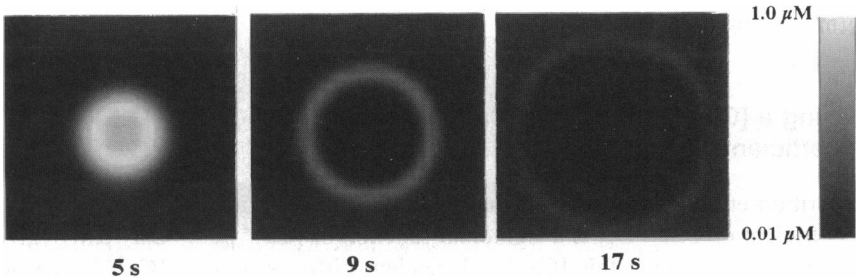

FIGURE 9 Circular wave induced by IP_3 release. Simulation result on a domain of dimensions 250 × 250 μm that is initially at a steady state $[Ca^{2+}]_c$ of 100 nM. $[IP_3]$ is raised to 2.5 μM for 300 ms on a square region with sides of 30 μm in the center of the domain, while $[IP_3]$ is initially 0 μM elsewhere. A circular wave is initiated from the region of elevated $[IP_3]$ but dies away within a radial distance of 100 μm. There is a relatively fast breakdown of IP_3 in this simulation (k_p = 0.2 s^{-1}).

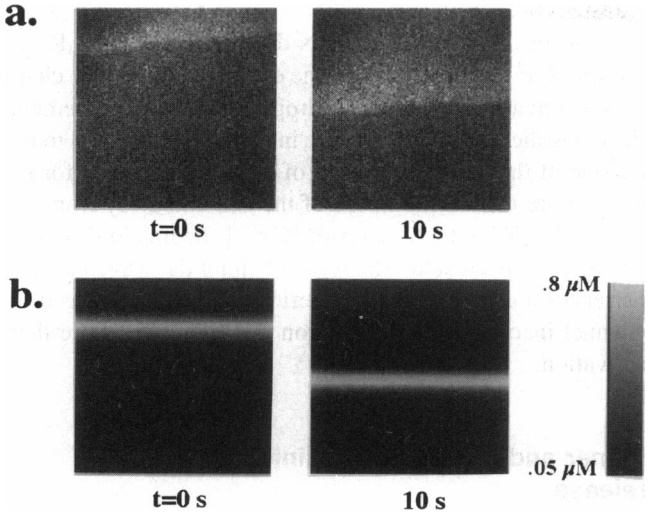

FIGURE 10 (*A*) Planar Ca^{2+} wave in the *Xenopus* oocyte. The images are 420 × 420 μm, and the signal is measured from a 40-μm slice at the surface of the oocyte. Images have not been filtered or subtracted. The velocity of this wave is 13 $\mu m \cdot s^{-1}$. Intracellular Ca^{2+} levels were imaged in oocytes of albino *Xenopus laevis* toads as described previously (Girard et al., 1992). Briefly, oocytes were manually defolliculated from surgically obtained ovarian lobes and microinjected with 50 nl of 0.25 mM calcium green dye. Ca^{2+} transients were stimulated by microinjection of the IP_3 analogue 3-deoxy IP_3 (a gift of Dr. A. Kozikowski) to give a final concentration of 0.5 μM. Images were collected at 1 Hz with a Biorad MRC-600 confocal microscope. (*B*) Simulation on a domain of dimensions 250 × 250 μm with a $[IP_3]$ of 95 nM across the whole domain. $[Ca^{2+}]_c$ is raised to 2.0 μM, for 6 s, on a rectangular region of width 30 μm on the whole upper part of the domain, while $[Ca^{2+}]_c$ is initially 129 nM elsewhere. A planar propagating wave of Ca^{2+} is initiated from the region of elevated $[Ca^{2+}]_c$ and travels across the domain.

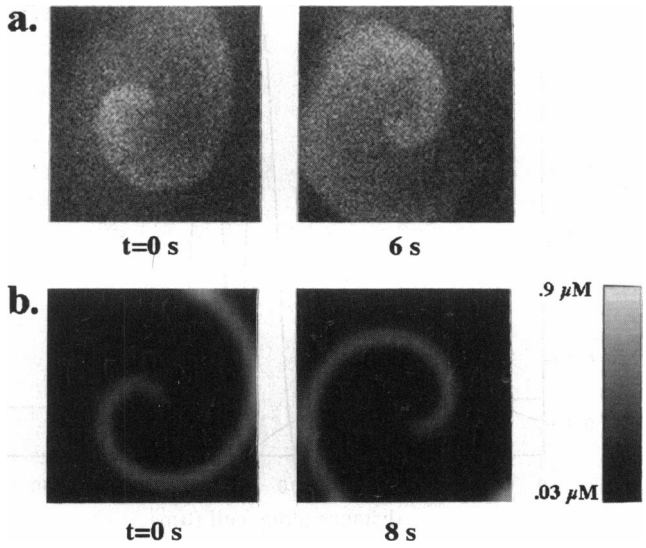

FIGURE 11 (*A*) Spiral Ca^{2+} wave in the *Xenopus* oocyte. The image size is 420 × 420 μm, and the signal is measured from a 40-μm slice at the surface of the oocyte. The rotational period of the spiral is about 12 s/rotation. (B) Simulation result on a domain of dimensions 250 × 250 μm with a $[IP_3]$ of 95 nM across the whole domain. A spiral wave results when part of a circular wave front of Ca^{2+} encounters a rectangular region of low $[Ca^{2+}]_c$ ($[Ca^{2+}]_c$ = 20 nM). Initially the whole domain has a steady-state $[Ca^{2+}]_c$ of 129 nM except for a small square region with a $[Ca^{2+}]_c$ of 920 nM, which is used to induce the circular wave, and a small rectangular (refractory) region of $[Ca^{2+}]_c$.

shows an observed spiral from a *Xenopus* oocyte and a spiral produced by a model simulation.

Dependence of wave speed and baseline $[Ca^{2+}]_c$ on Ca^{2+} influx

Girard and Clapham (1993) observed both an acceleration of Ca^{2+} wave speed and an increase in baseline $[Ca^{2+}]_c$ with increased influx of Ca^{2+} from outside the cell. We simulated increased influx of Ca^{2+} into the cytosol from the outside by increasing β, the constant influx rate of Ca^{2+} from the outside. Not surprisingly, baseline $[Ca^{2+}]_c$ increased with increasing β. Interestingly, we also found the wave speed to be an increasing function of β. As we varied β from 0 to 20 $nM \cdot s^{-1}$, the mean wave speed increased from 11.1 to 13.1 $\mu m \cdot s^{-1}$ (Fig. 12).

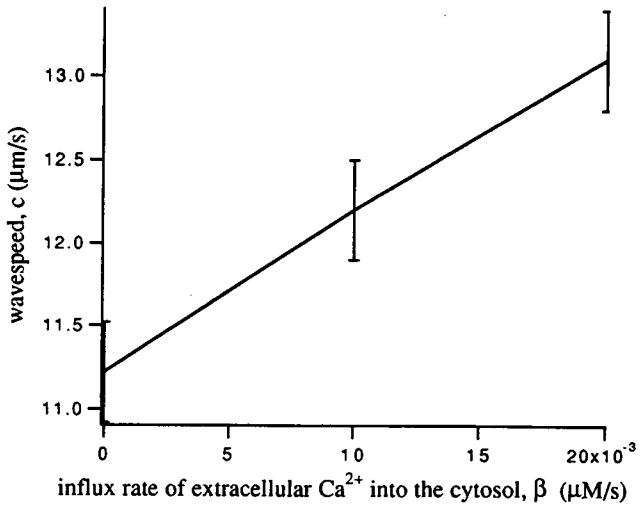

FIGURE 12 Acceleration of wave speed with increased influx of Ca^{2+} into the cytosol. Planar wave speed ($\mu m \cdot s^{-1}$) versus the rate of extracellular Ca^{2+} influx into the cytosol, β ($\mu M \cdot s^{-1}$). Error bars are centered at mean calculated wave speed. A numerical uncertainty of $\pm 0.3\ \mu m \cdot s^{-1}$ in the wave speed is a result of the discretization of the model equations. The least-square best-fit line to the data is shown.

Using a $[Ca^{2+}]_c$-dependent Ca^{2+} diffusion coefficient

Albritton et al. (1992) suggest that the cytosolic diffusion coefficient of Ca^{2+}, D_c, is a sigmoidal function of $[Ca^{2+}]_c$. Letting $D_c(c)$ denote this $[Ca^{2+}]_c$-dependent diffusion coefficient, we found that

$$D_c(c) = c_0 + \frac{D_{max} c^2}{k_c + c^2} \qquad (12)$$

with c_0 = 10 $\mu m^2 \cdot s^{-1}$, D_{max} = 200 $\mu m^2 \cdot s^{-1}$, and k_c = 2.5 μM^2 gives a reasonable fit to their data. This $[Ca^{2+}]_c$-dependent diffusion coefficient had very little effect

on the model's behavior. There was little change in either the wave speed or profile. During a model wave, the peak $[Ca^{2+}]$ is about 0.8 μM. Thus, during passage of a wave, D_c varies from about 10 to 50 $\mu m^2 \cdot s^{-1}$.

DISCUSSION

Our model serves as a minimal model of intracellular Ca^{2+} oscillations and waves in the *Xenopus laevis* oocyte. It captures the essential macroscopic elements sufficient to produce the wide range of spatiotemporal behaviors of Ca^{2+} inside the *Xenopus* oocyte. Our model thus shows the sufficiency of the following three characteristics in producing temporal oscillations of Ca^{2+}: (*a*) a single IP_3-sensitive intracellular pool of Ca^{2+}; (*b*) the biphasic dependence of the IP_3R on $[Ca^{2+}]_c$; (*c*) the separation of time scales for IP_3R activation and inactivation. The model not only displays the characteristic oscillatory behavior of *Xenopus* oocytes but also gives good agreement with the experimental results of Finch et al. (1991), Parker and Ivorra (1990), and Iino and Endo (1992). The model also displays excitability and mimics CICR in Ca^{2+} activation of the IP_3R and, to a lesser extent, in the lag in channel inactivation compared to activation.

For an appropriate range of $[IP_3]$, oscillations of $[Ca^{2+}]_c$ occur at a constant $[IP_3]$. Below this oscillatory range $[Ca^{2+}]_c$ is virtually unaltered by $[IP_3]$, while above this range there is a sustained elevation of $[Ca^{2+}]_c$ rather than oscillations (Berridge and Irvine, 1989). Also in accord with experimental evidence, the frequency and latency of the oscillations, respectively, increase and decrease as $[IP_3]$ increases, and the latency of the oscillations (the interval from stimulation to first spike) is a linear function of the period, with a slope of 2. In agreement with the experimental results of Finch et al. (1991), the model predicts that for fixed $[Ca_i^{2+}]$, IP_3-induced Ca^{2+} efflux is initially increased but decreases more rapidly for larger $[Ca^{2+}]_c$. Also, in agreement with the results of Parker and Ivorra (1990), the model predicts that following a pulse of IP_3, Ca^{2+} release from the pool, as a result of a second identical pulse, is greatly inhibited in the time range of 2.5–5 s but gradually recovers from this inhibition. Finally, simulation results agree with the experiments of Iino and Endo (1992), which analyze the kinetics of caged IP_3-induced Ca^{2+} release following the flash photolysis of caged IP_3 or caged Ca^{2+} and demonstrate that Ca^{2+}-dependent immediate feedback control is an important determinant of the time course of Ca^{2+} release.

The model of $[Ca^{2+}]_c$ oscillations (i.e., the temporal model) can then be used as a basis for a spatially extended model for $[Ca^{2+}]_c$ waves (i.e., a spatiotemporal model). Thus, our model for $[Ca^{2+}]_c$ oscillations was extended to two spatial dimensions, with the inclusion of IP_3 dynamics, cytosolic diffusion of IP_3 with a diffusion coefficient of 300 $\mu m^2 \cdot s^{-1}$, and cytosolic diffusion of Ca^{2+} with a diffusion coefficient of 20 $\mu m^2 \cdot s^{-1}$. Model simulations produce many of the observed spatiotemporal patterns of $[Ca^{2+}]_c$ in the *Xenopus* oocyte, including circular, planar, and spiral traveling waves of Ca^{2+}, which annihilate upon collision (Lechleiter and Clapham, 1992). Waves can be produced by increases of cytosolic $[IP_3]$ or by increases in $[Ca^{2+}]_c$ when a certain baseline $[IP_3]$ has primed the IP_3R for excitable release of Ca^{2+}. Also, in agreement with experimental data (Girard and Clapham, 1993), increasing extracellular $[Ca^{2+}]$ influx accelerates the wave speed and increases the baseline $[Ca^{2+}]_c$. Making the cytosolic diffusion coefficient of Ca^{2+} dependent on $[Ca^{2+}]_c$ (Albritton et al., 1992) does not affect the qualitative behavior of the model. Our model of Ca^{2+} waves is, therefore, a quantitative realization of the model of Lechleiter and Clapham (1992), who propose that biphasic modulation of the IP_3R by $[Ca^{2+}]_c$ and a relatively faster cytosolic diffusion of IP_3 compared to Ca^{2+} are the major elements responsible for the generation and propagation of Ca^{2+} waves inside the *Xenopus* oocyte.

An advantage of our model is that it can very easily be adapted to produce a model of intracellular $[Ca^{2+}]_c$ oscillations and wave propagation in any cell that uses the IP_3R as its primary source for release of Ca^{2+} into the cytosol. Once the biphasic dependence of IP_3R activation on $[Ca^{2+}]_c$ is determined experimentally, this information can be incorporated into the model, in the same way the data from *Xenopus* were, to produce an accurate model for the cell type under consideration.

One model prediction is that IP_3R inactivation must occur on a slower time scale than activation in order for $[Ca^{2+}]_c$ waves to propagate. This lag in inactivation compared to activation is not necessary to produce $[Ca^{2+}]_c$ oscillations but seems to be very necessary to propagating the $[Ca^{2+}]_c$ wave. Thus, whereas the channel dynamics plays a less integral role in the production of oscillations, it seems to play a crucial role in the spatial propagation of the Ca^{2+} signal. This prediction stresses the importance of the dynamics of the channel in propagating the Ca^{2+} signal.

The model also predicts a difference between the experiments in which IP_3 and IP_3S_3 are used to propagate Ca^{2+} waves. Since IP_3S_3 is not degraded it should support wave activity (from pulsating foci or regions) for a greater length of time. This is seen in model simulations (comparing simulations with $k_p = 0$ and $k_p > 0$).

APPENDIX

The single channel model

Our model is based on the following simplified model of a single IP_3R. It must be emphasised that, although the model is described in terms of specific physical processes, it is essentially phenomenological. The analogy with physical mechanisms should not be given undue weight. We make the following assumptions about the IP_3R:

1. The IP_3R consists of three independent binding domains, each of which may be in an activated or an unactivated state. We do not claim that each of these domains corresponds to a single binding site—for instance, 2 Ca^{2+} ions may bind cooperatively to different sites in domain 3. These domains are merely a convenient way to group the physical binding sites on the basis of functionality.

2. Domain 1 binds IP_3, whereas domains 2 and 3 bind Ca^{2+}. In order to fit the experimental data, we shall assume that one IP_3 binds to domain

1, one Ca^{2+} binds to domain 2, but two Ca^{2+} bind cooperatively to domain 3. This is discussed later.

3. The IP_3R will pass Ca^{2+} current only if domains 1 and 2 are activated and domain 3 is unactivated. Thus, activation of domains 1 and 2 will increase the Ca^{2+} flux, but activation of domain 3 will decrease the Ca^{2+} flux. It follows that, since Ca^{2+} binds to both domains 2 and 3, it can act to either increase or decrease the Ca^{2+} flux, depending on the domain to which it binds.

4. Even when $[IP_3]$ and $[Ca^{2+}]_c$ are zero, there is a nonzero probability that domains 1 and 2 will spontaneously activate. This is equivalent to assuming a basal current through the IP_3R. However, this assumption may be easily relaxed.

5. The Ca^{2+} current through the IP_3R is all or nothing. The total Ca^{2+} flux from the internal pool into the cytoplasm is controlled by the number of open channels.

With these assumptions, it follows that the probability that an individual channel is open is given by $p_1p_2p_3$, where p_1 and p_2 are the probabilities that domains 1 and 2, respectively, are activated, and p_3 is the probability that Ca^{2+} is not bound to domain 3 (unactivated). Thus, given a population of N channels, the total steady-state calcium current through the IP_3Rs, I, as a function of the Ca^{2+} and IP_3 concentrations is given by

$$I = Nip_1p_2p_3,$$

where i is the Ca^{2+} current through a single open channel and has units of $\mu C \cdot s^{-1}$. By assuming a constant volume, U, we can convert the Ca^{2+} current to a concentration flux, $J_{channel}$, where

$$J_{channel} = \frac{Nip_1p_2p_3}{2\mathcal{F}U},$$

where $\mathcal{F}$ is Faraday's constant, with units of coulombs per mole. Finally, we write $k_{flux} = Ni/(2\mathcal{F}U)$ to get

$$J_{channel} = k_{flux}p_1p_2p_3.$$

In our model, k_{flux} and $J_{channel}$ have units of $\mu M \cdot s^{-1}$.

We model p_1, p_2, and p_3 as functions of $[IP_3]$ and $[Ca^{2+}]_c$ by assuming cooperative kinetics (with Hill coefficients of 1, 1, and 2, respectively). Thus, if we let c denote $[Ca^{2+}]_c$ and P denote $[IP_3]$ then the following equations result:

$$p_1 = \mu_0 + \frac{\mu_1 P}{k_\mu + P} \tag{13}$$

$$p_2 = b + \frac{V_1 c}{k_1 + c} \tag{14}$$

$$p_3 = 1 - \frac{c^2}{k_2^2 + c^2}. \tag{15}$$

Hence, at the steady state

$$J_{channel} = k_{flux}\left(\mu_0 + \frac{\mu_1 P}{k_\mu + P}\right)\left(b + \frac{V_1 c}{k_1 + c}\right)\left(1 - \frac{c^2}{k_2^2 + c^2}\right). \tag{16}$$

It is important to note that this is a steady-state relationship only. Equations 14 and 15 are phenomenological: they were not constructed from consideration of fundamental processes, but merely to agree with the data of Parys et al. (1992) from the IP_3R of *Xenopus* oocytes (the curve is shown in Fig. 2 *a*). Equation 16 is, therefore, not a model prediction but was constructed directly from consideration of the experimental data. The steady-state proportion of channels with domain 2 activated is represented by a Hill function with an exponent of 1 plus a small leak term. This serves to account for the rising part of the bell-shaped curve and for the asymmetry that has the left side of the curve elevated compared to the right side (i.e., even at very low $[Ca^{2+}]_c$ there is a relatively substantial flux of Ca^{2+} through the channel as compared to very high $[Ca^{2+}]_c$) (Fig. 2 *b*). Meanwhile, the steady-state proportion of channels with domain 3 unactivated, $p_3(c)$, involves Ca^{2+} cooperativity and acts as a negative feedback on the release process, and thus, analogously, it is represented by a reverse Hill function with an exponent of 2.

Although this is a less detailed construction than some previous models have used (DeYoung and Keizer, 1992), it has some compensating advantages, including ease of construction and modification for use in a wide variety of cell types.

Dynamic behavior of the channel

For a fixed $[Ca^{2+}]_c$ the steady flux through the channel is given by Eq. 16, but we have not yet specified how the channel responds to a changing $[Ca^{2+}]_c$. It turns out that this dynamic behavior is a crucial component of the overall Ca^{2+} response. Experimental data (Finch et al., 1991) indicate that when $[Ca^{2+}]_c$ is suddenly increased, the IP_3R quickly activates and then, more slowly, deactivates. We thus assume that binding domains 1 and 2 reach a fast equilibrium with IP_3 and $[Ca^{2+}]_c$, but that domain 3 relaxes to its steady state with time constant τ_n. If for notational convenience we use n in place of p_3, we can then write the rate of change of c due to Ca^{2+} flux through the IP_3R as

$$\frac{dc}{dt} = k_{flux}\left(\mu_0 + \frac{\mu_1 P}{k_\mu + P}\right)n\left(b + \frac{V_1 c}{k_1 + c}\right) \tag{17}$$

$$\tau_n \frac{dn}{dt} = 1 - \frac{c^2}{k_2^2 + c^2} - n. \tag{18}$$

The variable n in this model is analogous to the inactivation variable h in the Hodgkin-Huxley equations.

Finally, including a constant Ca^{2+} leak from the extracellular space into the cytoplasm and a Ca^{2+} pump that pumps Ca^{2+} out of the cytoplasm with saturable kinetics, we get the complete model for Ca^{2+} oscillations (Eqs. 1–7 in the text).

A. Atri is supported by National Institutes of Health grant 08135. D. Clapham is an Established Investigator of the American Heart Association and is supported by National Institutes of Health grant HL41303. J. Sneyd is supported by National Institutes of Health grant R29 GM48682-01.

REFERENCES

Albritton, N. L., T. Meyer, and L. Stryer. 1992. Range of messenger action of calcium ion and inositol 1,4,5-trisphosphate. *Science (Washington DC).* 258:1812–1815.

Berridge, M. J. 1985. The molecular basis of communication within the cell. *Sci. Am.* 253:142–152.

Berridge, M. J. 1987. Inositol trisphosphate and diacylglycerol: two interacting second messengers. *Annu. Rev. Biochem.* 56:159–193.

Berridge, M. J. 1993. Inositol trisphosphate and calcium signalling. *Nature (Lond.).* 361:315–325.

Berridge, M. J., and A. Gallione. 1988. Cytosolic calcium oscillators. *FASEB J.* 2:3074–3082.

Berridge, M. J., and R. F. Irvine. 1989. Inositol phosphates and cell signalling. *Nature (Lond.).* 341:197–205.

Bezprozvanny, I., J. Watras, and B. E. Ehrlich. 1991. Bell-shaped calcium-response curves of $Ins(1,4,5)P_3$- and calcium-gated channels from endoplasmic reticulum of cerebellum. *Nature (Lond.).* 351:751–754.

Boitano, S., E. R. Dirksen, and M. J. Sanderson. 1992. Intercellular propagation of calcium waves mediated by inositol trisphosphate. *Science (Washington DC).* 258:292–295.

Camacho, P., and J. D. Lechleiter. 1993. Increased frequency of calcium waves in *Xenopus laevis* oocytes that express a calcium-ATPase. *Science (Washington DC).* 260:226–229.

Carafoli, E. 1987. Intracellular calcium homeostasis. *Annu. Rev. Biochem.* 56:395–433.

Charles, A., J. E. Merrill, E. R. Dirksen, and M. J. Sanderson. 1991. Intercellular signalling in glial cells: calcium waves and oscillations in response to mechanical stimulation and glutamate. *Neuron.* 6:983–992.

Cobbold, P. H., and K. S. R. Cuthbertson. 1990. Calcium oscillations: phenomena, mechanisms and significance. *Semin. Cell Biol.* 1:311–321.

Cuthbertson K. S. R. 1989. Intracellular calcium oscillators. *In* Cell to Cell Signalling: From Experiments to Theoretical Models. A. Goldbeter, editor. Academic Press, London. 3–38.

Cuthbertson, K. S. R., and T. R. Chay. 1991. Modelling receptor-controlled intracellular calcium oscillators. *Cell Calcium.* 12:97–109.

Davis, T. N. 1992. What's new with calcium? *Cell.* 71:557–564.

DeLisle, S., and M. J. Welsh. 1992. Inositol trisphosphate is required for the propagation of calcium waves in *Xenopus* oocytes. *J. Biol. Chem.* 267: 7963–7966.

DeYoung, G. W., and J. Keizer. 1992. A single pool IP_3-receptor-based model for agonist stimulated Ca^{2+} oscillations. *Proc. Natl. Acad. Sci. USA.* 89:9895–9899.

Ehrenstein G., and R. FitzHugh. 1986. A channel model for development of the fertilization membrane in sea urchin eggs. *In* Ionic channels in cells and model systems. R. Latorre, editor. Plenum Publishing Corporation, New York.

Endo, M., M. Tanaka, and Y. Ogawa. 1970. Calcium induced release of calcium from the sarcoplasmic reticulum of skinned skeletal muscle fibres. *Nature (Lond.).* 228:34–36.

Fabiato, A. 1983. Calcium-induced release of calcium from the cardiac sarcoplasmic reticulum. *Am. J. Physiol.* 245:C1–C14.

Finch, E. A., T. J. Turner, and S. M. Goldin. 1991. Calcium as a coagonist of inositol 1,4,5-trisphosphate-induced calcium release. *Science (Washington DC).* 252:442–446.

Girard, S., and D. Clapham. 1993. Acceleration of intracellular calcium waves in *Xenopus* oocytes by calcium influx. *Science (Washington DC).* 260:229–232.

Girard S., A. Lückhoff, J. Lechleiter, J. Sneyd, and D. Clapham. 1992. Two-dimensional model of calcium waves reproduces the patterns observed in *Xenopus* oocytes. *Biophys. J.* 61:509–517.

Goldbeter, A., G. Dupont, and M. J. Berridge. 1990. Minimal model for signal-induced calcium oscillations and for their frequency encoding through protein phosphorylation. *Proc. Natl. Acad. Sci. USA.* 87:1461–1465.

Harootunian, A. T., J. P. Y. Kao, and R. Y. Tsien. 1989. Agonist-induced calcium oscillations in depolarized fibroblasts and their manipulation by photoreleased $Ins(1,4,5)P_3$, Ca^{2+}, and Ca^{2+} buffer. *Cold Spring Harbor Symp. Quant. Biol.* 53:935–943.

Hodgkin, A. L., and A. F. Huxley. 1952. A quantitative description of membrane current and its application to conduction and excitation in nerve. *J. Physiol.* 117:500–544.

Iino, M. 1990. Biphasic Ca^{2+} dependence of inositol 1,4,5-trisphosphate-induced Ca^{2+} release in smooth muscle cells of the guinea pig *Taenia caeci. J. Gen. Physiol.* 95:1103–1122.

Iino, M., and M. Endo. 1992. Calcium-dependent immediate feedback control of inositol 1,4,5-trisphosphate-induced Ca^{2+} release. *Nature (Lond.).* 360:76–78.

Keener, J. P. 1986. A geometrical theory for spiral waves in excitable media. *SIAM J. Appl. Math.* 46:1039–1056.

Keizer, J., and G. DeYoung. 1993. Simplification of a realistic model of IP_3-induced Ca^{2+} oscillations. *J. Theor. Biol.* in press.

Lechleiter, J. D., and D. E. Clapham. 1992. Molecular mechanisms of intracellular calcium excitability in *X. laevis* oocytes. *Cell.* 69:283–294.

Lytton, J., M. Westlin, S. E. Burk, G. E. Shull, and D. H. MacLennan. 1992. Functional comparisons between isoforms of the sarcoplamic or endoplasmic reticulum family of calcium pumps. *J. Biol. Chem.* 267:14483–14489.

Meyer, T., and L. Stryer. 1991. Calcium spiking. *Annu. Rev. Biophys. Chem.* 20:153–174.

Murray, J. D. 1989. Mathematical Biology. Springer Verlag, New York. pp 161–166, ch. 11–12.

Parker, I., and I. Ivorra. 1990. Inhibition by Ca^{2+} of inositol trisphosphate-mediated Ca^{2+} liberation: a possible mechanism for oscillatory release of Ca^{2+}. *Proc. Natl. Acad. Sci. USA.* 87:260–264.

Parker, I., and I. Ivorra. 1992. Characteristics of membrane currents evoked by photoreleased inositol trisphosphate in *Xenopus* oocytes. *Am. J. Physiol.* 263:C154–C165.

Parker, I., and Y. Yao. 1992. Regenerative release of calcium from functionally discrete subcellular stores by inositol trisphosphate. *Proc. R. Soc. Lond. B Biol.* 246:269–274.

Parys, J. B., S. W. Sernett, S. DeLisle, P. M. Snyder, M. J. Welsh, and K. P. Campbell. 1992. Isolation, characterization, and localization of the inositol 1,4,5-trisphosphate receptor protein in *Xenopus laevis* oocytes. *J. Biol. Chem.* 267:18776–18782.

Peterson, O. H., and M. Wakui. 1990. Oscillating intracellular calcium signals evoked by activation of receptors linked to inositol lipid hydrolysis: mechanism of generation. *J. Membr. Biol.* 118:93–105.

Quin, S. J., G. H. Williams, and D. L. Tillotson. 1988. Calcium oscillations in single adrenal glomerulosa cells stimulated by angiotensin II. *Proc. Natl. Acad. Sci. USA.* 85:5754–5758.

Rooney, T. A., E. J. Sass, and A. P. Thomas. 1990. Characterization of cytosolic calcium oscillations induced by phenylephrine and vasopressin in single fura-2-loaded hepatocytes. *J. Biol. Chem.* 264:17131–17141.

Sage, S. O., and T. J. Rink. 1987. The kinetics of changes in intracellular calcium concentration in fura-2-loaded human platelets. *J. Biol. Chem.* 262:16364–16369.

Sanderson, M. J., A. C. Charles, and E. R. Dirksen. 1990. Mechanical stimulation and intercellular communication increases intracellular Ca^{2+} in epithelial cells. *Cell Regul.* 1:585–596.

Sneyd, J., and A. Atri. 1993. Curvature dependence of a model for calcium wave propagation. *Physica D.* 65:365–372.

Sneyd, J., and L. Kalachev. 1993. A profile analysis of propagating calcium waves. *Cell Calcium.* In press.

Sneyd J., S. Girard, and D. Clapham. 1992. Calcium wave propagation by calcium-induced calcium release: an unusual excitable system. *Bull. Math. Biol.* 55:315–344.

Somogyi, R., and J. W. Stucki. 1991. Hormone-induced calcium oscillations in liver cells can be explained by a simple one pool model. *J. Biol. Chem.* 266:11068–11077.

Tsien, R. W., and R. Y. Tsien. 1990. Calcium channels, stores, and oscillations. *Annu. Rev. Cell Biol.* 6:715–760.

Tsunoda, Y. 1991. Oscillatory calcium signalling and its cellular function. *New Biologist.* 3:3–17.

Zykov, V. S. 1980. Analytical evaluation of the dependence of the speed of an excitation wave in a two-dimensional excitable medium on the curvature of its front. *Biophys. J.* 25:906–911.